



Effect of Gadolinium Doping on the Structure of $Ce_{1-x}Gd_xO_{2-x/2}$ Solid Solutions Prepared by Ionic Gelation Approach

V. Ilcheva ^{1*}, V. Boev ¹, E. Lefterova ¹, G. Avdeev ², O. Dimitrov ¹,
N. Bojanova ¹, H. Kolev ³, T. Petkova ¹

¹ Institute of Electrochemistry and Energy Systems "Academician Evgeni Budevski", Bulgarian Academy of Sciences, 1113 Sofia, Bulgaria.

² Institute of Physical Chemistry "Academician Rostislav Kaischew", Bulgarian Academy of Sciences, 1113 Sofia, Bulgaria.

³ Institute of Catalysis, Bulgarian Academy of Sciences, 1113 Sofia, Bulgaria.

Abstract

The current research aims to present the structural characterization of Gd-doped ceria powders and ceramics, investigating the structural evolution resulting from cerium substitution with Gd across the entire composition range from 0 to 100 mol.% Gd_2O_3 . $Ce_{1-x}Gd_xO_{2-x/2}$ powders with varying Gd contents ($0 \leq x \leq 1$) were synthesized using the ionic gelation method followed by thermal annealing. The resulting powders were subjected to high-temperature treatment to obtain ceramics. Characterization methods included X-ray diffraction (XRD) to identify phase composition and confirm the formation of $Ce_{1-x}Gd_xO_{2-x/2}$ solid solutions, infrared spectroscopy (IR) and scanning electron microscopy (SEM) for structural and morphological studies, and X-ray photoelectron spectroscopy (XPS) to evaluate the electronic structure. Comparative analysis of Gd-doped calcined powders and sintered pellets revealed the impact of thermal treatment on the structural features of the resulting solid solutions, elucidating the influence of gadolinium substitution. The novelty of this research lies in demonstrating the successful preparation of $Ce_{1-x}Gd_xO_{2-x/2}$ solid solutions via an alginate-mediated ion-exchange process and providing a detailed structural investigation over the entire range of dopant concentrations. This assessment highlights the feasibility for further research of these materials as suitable candidates for intermediate-temperature solid oxide fuel cells (IT-SOFCs) or catalyst applications.

Keywords:

Cerium Oxide;
Gadolinium;
Ionic Gelation Method;
XPS;
Ceramics.

Article History:

Received:	30	April	2024
Revised:	28	August	2024
Accepted:	06	September	2024
Published:	01	October	2024

1- Introduction

Cerium oxide (CeO_2) has provoked considerable attention in the recent years due to its unique properties and diverse application areas, particularly in the field of green energy technologies, which are very relevant today [1]. The possibility to modify its physicochemical properties through doping with different elements opens up opportunities for fine-tuning important characteristics of CeO_2 -based materials to meet specific application requirements, particularly in energy conversion [2] and storage systems [3]. Extensive research has been directed toward studying the effect of doping CeO_2 with various rare earth elements embedded into the cerium oxide lattice to enhance its performance as an electrolyte material in solid oxide fuel cells (SOFCs) [4-8] and in particular such operating at intermediate temperatures (500–700°C) (IT SOFCs), due to their high ionic conductivity in this temperature range [9, 10].

Among the investigated aliovalent dopants, gadolinium emerged as a promising candidate for improving the functional characteristics of CeO_2 -based materials for the aforementioned applications. Substitution of Ce^{4+} with an

* **CONTACT:** vania.ilcheva@iees.bas.bg

DOI: <http://dx.doi.org/10.28991/ESJ-2024-08-05-01>

© 2024 by the authors. Licensee ESJ, Italy. This is an open access article under the terms and conditions of the Creative Commons Attribution (CC-BY) license (<https://creativecommons.org/licenses/by/4.0/>).

appropriate amount of trivalent rare earth elements such as Gd^{3+} in the cationic sublattice creates oxygen vacancies through charge compensation, promoting the diffusion of oxygen atoms in the CeO_2 crystal lattice. This contributes to the increasing ionic conductivity of the obtained gadolinium substituted cerium oxides and facilitates their use as electrolyte material for IT SOFC application [1, 11, 12].

Despite significant progress in the research results currently available in the literature focused on the study and analysis of the general structural properties of Gd-doped ceria oxides, there remain some gaps related to the insufficient availability of comprehensive analyses that correlate these properties with different Gd concentrations spanning the entire range of compositions - from 0 to 100 mol. % rare earth dopant concentration. In general, the rare-earth-doped cerium oxides obtained by the sol-gel method at a relatively low synthesis temperature (about 500 °C), compared to the conventional high-temperature method (about 1300 °C), have not been sufficiently studied in a wide concentration range. Moreover, the influence of subsequent heat treatment on the structural and electronic properties of such oxide materials has not been extensively explored to date.

Considering the above, the aim of the present work is to fill these gaps by providing a detailed structural characterization of Gd-doped CeO_2 powders and ceramics synthesized using an ionic gelation method, combined with thermal treatment at different temperatures. The evolution of the structure as a function of Gd content, ranging from 0 to 100 mol.% Gd_2O_3 , and the impact of the performed thermal treatment are investigated and discussed.

The research direction towards elucidating the complex relationship between rare-earth dopant concentration and the structural properties of the obtained solid oxides will contribute to the development of advanced ceria-based materials with tailored properties such as improved oxygen storage capacity [13], redox properties [14, 15] and catalytic activity [16-18] determining the possibilities of their use as materials for various technological applications.

The structure of the article is as follows: After the introductory section, the second part describes in detail the materials and methods used in this study. To better visualize the experimental procedure, this section includes a flowchart of the experimental process along with selected photos of the obtained materials. The results and their interpretation are then presented in the discussion section, which provides a detailed insight into the structural characterization of the synthesized materials. Finally, the last section summarizes the main conclusions and suggests potential future practical benefits of our research.

2- Material and Methods

A flowchart of the experimental procedure with pictures of the products at each stage of the synthesis is presented in Figure 1. $Ce_{1-x}Gd_xO_{2-x/2}$ ($0 \leq x \leq 1$) powders were synthesized by the ionic gelation (IG) method, which involves mixing an initial solution of 2 wt% sodium alginate, low viscosity ($C_6H_7O_7$)A($C_6H_7O_7$)BNa, (ThermoFisher Scientific Ltd., UK) as a gelling agent, with preliminary prepared aqueous solutions of $Ce(NO_3)_3 \cdot 6H_2O$, 99.99 % and $Gd(NO_3)_3 \cdot 6H_2O$, 99.99%, (Sigma-Aldrich, USA) in appropriate proportions, followed by thermal annealing of the resulting gel at a temperature of 500 °C. The preparation procedure is described in details in Pezeshkpour et al. [19] and Wang et al. [20]. The obtained powder samples (referred to as low temperature samples (LT) further in the text) were pressed into pellets (34 MPa) and sintered at 1400 °C for 3 h to produce ceramics (referred to as high temperature samples (HT) further in the text).

The phase composition and the identification of $Ce_{1-x}Gd_xO_{2-x/2}$ solid solution formation were accomplished by X-ray diffraction (XRD) using a Philips X-ray diffractometer PW 1030 with an X-ray source of Cu K α radiation ($\lambda = 1.5406 \text{ \AA}$) and θ -2 θ Bragg-Brentano geometry. The scan step size was 0.03°, the collection time - 1s and the 2 θ range was 5-90°. Interpretation of the diffraction patterns was carried out using the database PDF 2 - 2022, ICDD. The lattice parameters were determined by peak profile and position fitting of the XRD data by Pawley method [21].

The morphology of LT and HT samples was characterized by scanning electron microscopy using Scanning electron microscope PHILIPS SEM 515. The images were taken at 8 kV accelerating voltage using secondary electrons signal.

The basic structural units in the obtained materials were determined by Fourier-transform infrared spectroscopy using Bruker Tensor 27 spectrometer. The samples were examined in the form of discs with a thickness of about 0.25 mm, prepared by pressing a solid mixture of finely ground sample and KBr. The spectra were collected with 64 scans at a resolution of 2 cm^{-1} , referring to the air as a background spectrum for better accuracy.

The electronic structure of the powders and ceramics was identified by X-ray photoelectron spectroscopy (XPS). The measurements were performed by an ESCALAB MkII (VG Scientific, now Thermo Scientific) spectrometer equipped with a double-anode MgK α /AlK α nonmonochromic X-ray source with excitation energies of 1253.6 and 1486.6 eV. The energy scale was calibrated by normalizing the C1s line of the random hydrocarbons to 285.0 eV for electrostatic charging of the sample. Binding energies were determined by measuring the O 1s, Ce 3d, Gd 3d, Gd 4d, and Na 1s photoelectron peaks. Peak positions and areas were estimated by fitting a symmetric Gauss-Lorentz curve.

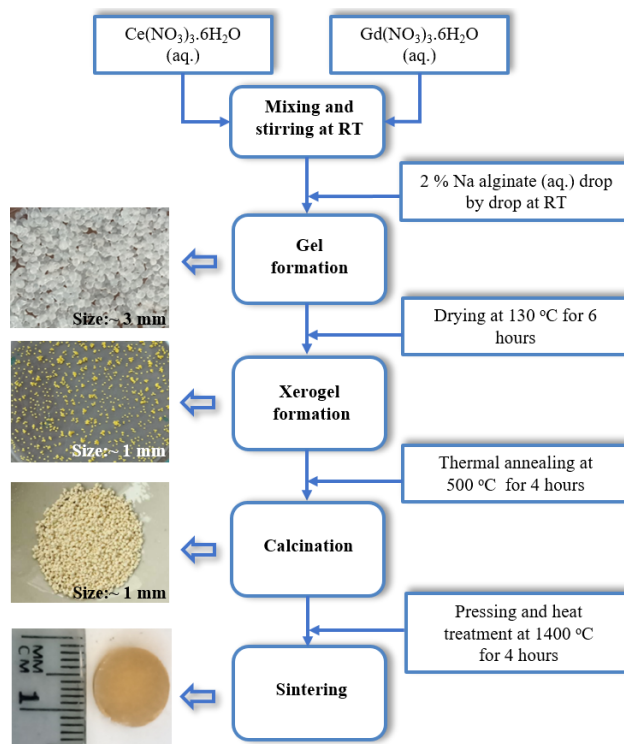


Figure 1. Flowchart of the experimental procedure with pictures of the products at each stage of the synthesis

3- Results and Discussion

3-1- XRD Characterization

The XRD patterns of the $Ce_{1-x}Gd_xO_{2-x/2}$ powders (LT samples) ($0 \leq x \leq 1$) are shown on Figure 3a. The observed relatively broad peaks suggest a crystallite size of several tens of nanometers, which is related to the relatively low temperature of post-treatment of the LT samples ($500^\circ C$). The broadening of the peaks with the increasing amount of gadolinium indicates defects accumulation as a result of the incorporation of a trivalent element into the CeO_2 lattice. A slight shift of the diffraction peaks of ceria towards lower 2θ is observed across the entire concentration range.

The interpretation of the diffractograms was performed using the PDF 2 - 2022 database, ICDD. The mineral Cerianite (ICSD 98-002-9046, ICDD #PDF 01-073-6328), which crystallizes in a CaF_2 structure, was used as the initial structural model. The lattice parameters, calculated using the Pawley method (as mentioned in the experimental section), and the crystallite size values of the calcined samples (LT) are presented in Table 1. Based on these calculations, it was established that in the concentration range $0.1 \leq x \leq 0.6$, cerium-gadolinium oxide crystallizes in a face-centered (FC) cubic lattice with space group $Fm-3m$. At $x > 0.6$, there is a transition from a face-centered to a body-centered (BC) cubic lattice with space group $Ia-3$. It is evident that the incorporation of gadolinium into the CeO_2 lattice leads to an increase in the lattice parameter, accompanied by a decrease in the average crystallite size, coinciding with the transition from the FCC to the BCC lattice. This transition is associated with the expansion of the unit cell of the cubic lattice due to the difference in the ionic radii of Ce^{4+} (0.97 \AA) and Gd^{3+} (1.04 \AA). Therefore, it is reasonable to expect an increase in the cubic lattice parameter of the fluorite-type phases upon the incorporation of Gd^{3+} .

Literature data indicate that the transition from FC to BC lattice for this system becomes noticeable when the Gd_2O_3 content exceeds 40 mol. % [22]. It is evident that for the samples obtained by the ion gelation method, the cubic FC lattice remains stable at $x = 0.6$. For the sake of clarity, Figure 3b presents the diffractograms for the concentration range $0.7 \leq x \leq 0.9$, indicating the transition from the FCC to the BCC lattice. As shown in the figure, the appearance of peaks characteristic to the $Ia-3$ space group is identified.

The aforementioned structural transition is illustrated in Figure 2, where structural models of CeO_2 (space group $Fm-3m$) and $Ce_{0.2}Gd_{0.8}O_{1.60}$ (space group $Ia-3$) are depicted. The modeling of the structures was performed using VESTA 3 software, which allows for three-dimensional visualization of crystal, volumetric, and morphology data [23].

From the structural model presented in Figure 2(b), it can be seen that the replacement of Ce^{4+} with Gd^{3+} results in deformation of the environment around the cations and oxygen atoms in the crystal lattice. Consequently, instead of a perfect cubic 8-coordinated environment for the cerium ion (as indicated in Figure 2(a)), deformation occurs along the cube diagonal.

Table 1. Structural characteristics of $Ce_{1-x}Gd_xO_{2-x/2}$ powders and ceramics determined by peak profile and position fitting of XRD data

Sample (empirical formula)	LT			HT	
	Space Group	Cell param. (Å)	Aver. size (Å)	Space Group	Cell param. (Å)
CeO_2	Fm-3m	5.411(9)	86	Fm-3m	5.410(3)
$Ce_{0.9}Gd_{0.1}O_{1.95}$	Fm-3m	5.418(3)	85,5	Fm-3m	5.417(1)
$Ce_{0.8}Gd_{0.2}O_{1.90}$	Fm-3m	5.426(0)	76	Fm-3m	5.422(6)
$Ce_{0.7}Gd_{0.3}O_{1.85}$	Fm-3m	5.432(9)	71	Fm-3m	5.427(5)
$Ce_{0.6}Gd_{0.4}O_{1.80}$	Fm-3m	5.436(7)	65	Ia-3	10.858(7)
$Ce_{0.5}Gd_{0.5}O_{1.75}$	Fm-3m	5.444(0)	50	Ia-3	10.855(5)
$Ce_{0.4}Gd_{0.6}O_{1.70}$	Fm-3m	5.451(6)	43	Ia-3	10.855(4)
$Ce_{0.3}Gd_{0.7}O_{1.65}$	Ia-3	10.89(6)	42	Ia-3	10.846(1)
$Ce_{0.2}Gd_{0.8}O_{1.60}$	Ia-3	10.88(7)	39	Ia-3	10.836(0)
$Ce_{0.1}Gd_{0.9}O_{1.55}$	Ia-3	10.86(4)	68	Ia-3	10.824(5)
					14.093(1)
Gd_2O_3	Ia-3	10.82(5)	180	C 1 2/m 1	3.574(9)
					8.764(1)

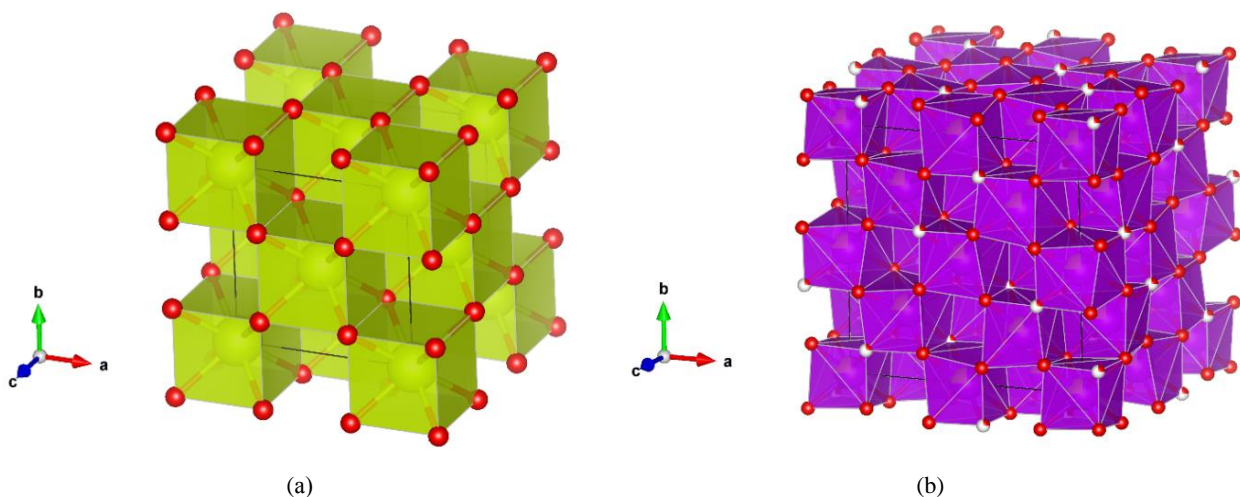


Figure 2. Crystal structure model of: a) CeO_2 (Fm-3m) in which cerium ions occupy the center of the cube formed by 8 oxygen ions; b) $Ce_{0.2}Gd_{0.8}O_{1.60}$ (Ia-3) in which the cerium and gadolinium ions share the same crystallographic position and are again located in an 8-coordinated oxygen polyhedron, representing a cube deformed along the volume diagonal (oxygen ions are indicated in red).

The stability of the FCC lattice over a broader concentration range could be attributed to: (1) the presence of linear defects, which act as compensatory centers around which Gd^{3+} ions accumulate; and (2) the compensation of Gd^{3+} charge by sodium impurities, the presence of which was confirmed by XPS and IR analyses (see below). These sodium ions do not have a specific location in the crystal lattice and their corresponding phase cannot be identified by X-ray phase analysis due to their relatively low concentration.

The diffractograms of the sintered ceramic samples (HT) are presented in Figure 4. As shown in the figure, high-temperature treatment of the $Ce_{1-x}Gd_xO_{2-x/2}$ powders leads to the sharpening of the XRD peaks, indicating an increase in the crystallinity of the ceramic structure (Figure 4a). Figure 4b demonstrates the appearance of new diffraction peaks associated with the formation of a body-centered cubic (BCC) cell as the gadolinium content increases.

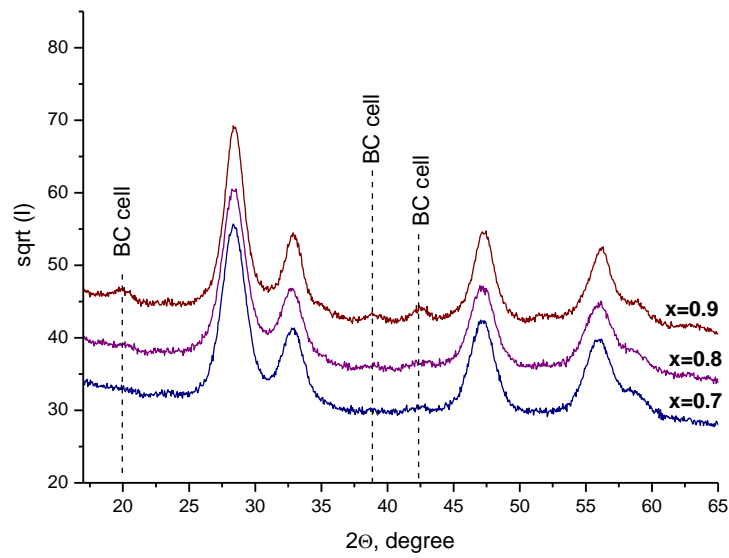
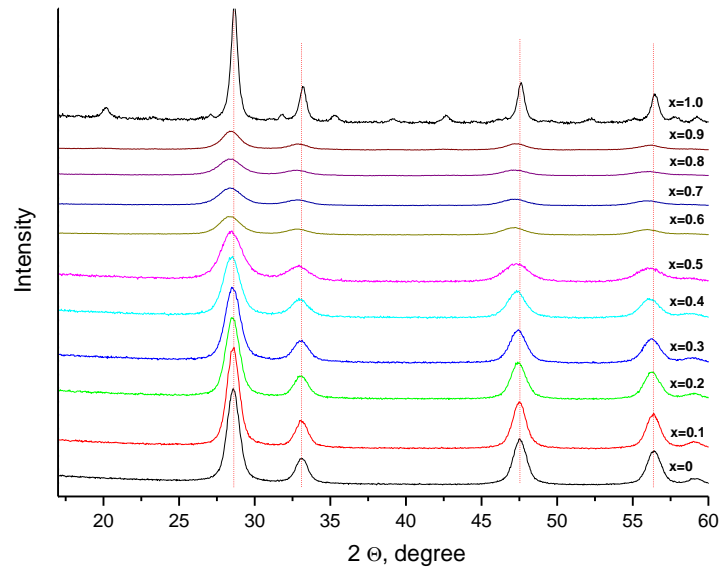
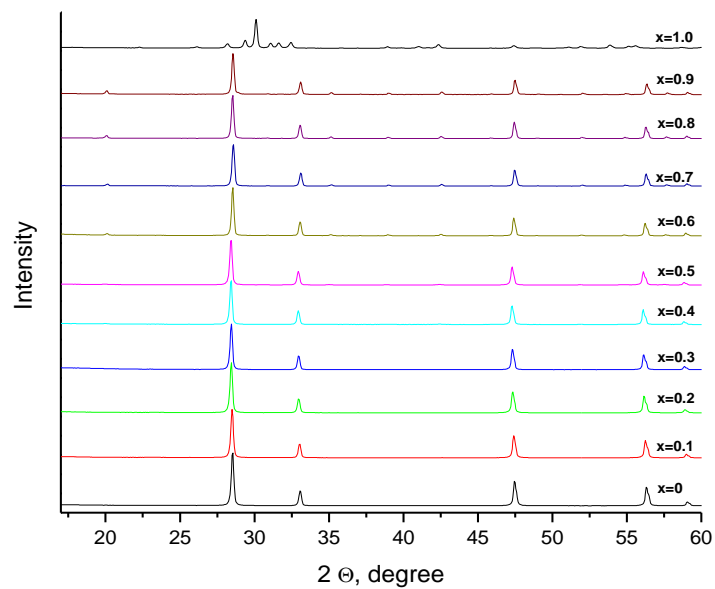


Figure 3. XRD patterns of $Ce_{1-x}Gd_xO_{2-x/2}$ powders (LT samples): a) in the entire composition range; b) in the range $0.7 \leq x \leq 0.9$



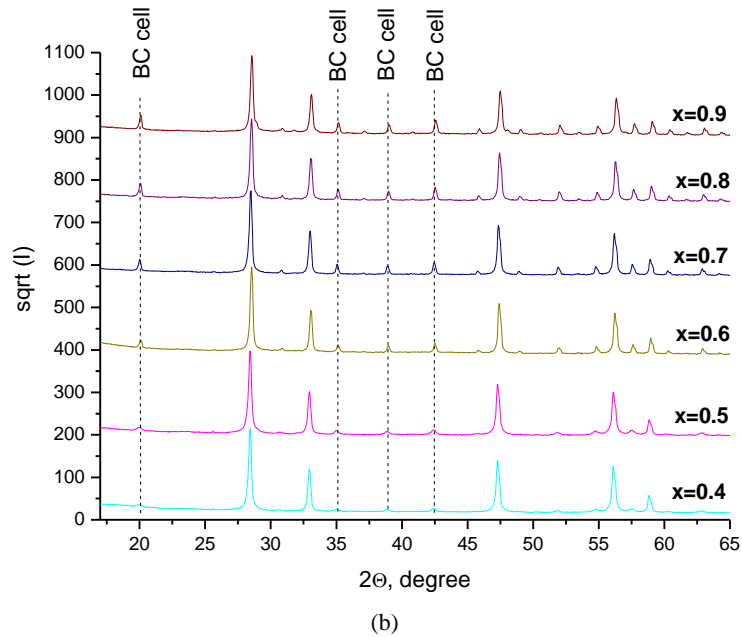


Figure 4. XRD patterns of the $\text{Ce}_{1-x}\text{Gd}_x\text{O}_{2-x/2}$ samples thermally treated at $1400\text{ }^\circ\text{C}$ and subsequently powdered: a) in the entire composition range; b) in the range $0.4 \leq x \leq 0.9$.

Evidently, the structural transformation from the Fm-3m to Ia-3 space group occurs at $x \geq 0.4$ in the HT samples, whereas in the LT powders, this transition occurs at $x \geq 0.7$. The coherent size of the crystallites in the LT samples, which is on the order of a few nanometers, indicates the presence of numerous structural defects in their crystal lattice. These defects contribute to the stabilization of the CaF_2 -type lattice over a wider range compared to what is observed in the HT samples. Judging from the full-width at half-maximum (FWHM) of the diffraction peaks, the coherent crystallite size in the HT samples is at least two orders of magnitude larger, although its exact value could not be determined due to peak broadening being very close to or even matching the instrumental broadening of the X-ray diffractometer used. The absence of sodium impurities in the crystal lattice, as evidenced by FTIR and XPS spectral analysis of the HT samples (see sections 3-3 and 3-4), facilitates the migration of other ions and accelerates the transformation of the crystal structure.

3-2- SEM study

The cross-section morphology images of $\text{Ce}_{1-x}\text{Gd}_x\text{O}_{2-x/2}$ ceramic pellets sintered at $1400\text{ }^\circ\text{C}$ are shown in Figure 5. The SEM analysis reveals a clear trend in the microstructural evolution of these ceramics with increasing of the Gd content. Specifically, the SEM images illustrate how the grain size and porosity change as a function of Gd doping, supporting the observed trend in the material's microstructural development. This trend confirms the assumption of the structural changes occurring and highlights the influence of Gd content on the densification and overall microstructure of the ceramics.

The SEM micrograph of the undoped CeO_2 ceramic sample ($x = 0$) clearly visualizes the rather non-compact microstructure characterized by grains with poorly formed boundaries as well as the presence of large intergranular pores. This indicates that the material has not achieved full densification, which may affect negatively its mechanical properties and ionic conductivity. As the Gd content increases to $x = 0.3$, there is a noticeable improvement in grain boundary formation. The particles begin to exhibit more defined shapes and the pore size distribution becomes more uniform. This intermediate level of doping suggests a partial enhancement in the densification of the material. The substitution of Ce by Gd up to $x = 0.5$ leads to the formation of more tightly packed irregularly shaped particles and also to a decrease in the size and number of intergranular pores. The observed significant reduction in particle size and more compact grain structure at this substitution level can be related to the structural transformation from Fm-3m space group to Ia-3 occurring in the ceramic samples at this additive concentration. This assumption is consistent with the results obtained from the XRD analysis as shown in Table 1 (HT samples). At higher doping level of $x = 0.7$, the SEM micrograph shows a further reduction in particle size and visualizes greater uniformity of grain shape and size. However, the microstructure still contains pores, suggesting that complete densification of the material structure has not been achieved. This insufficiently compact structure of the obtained ceramics could be related both to the specificity of the ionic gelation method that we used for the synthesis of the powder samples, and it could also be due to the insufficiently high pressure applied during the pressing of the ceramic pellets, subject to the present analysis.

The assumption of a correlation between SEM observations and structural XRD data supports the hypothesis that Gd doping improves the structural properties of CeO₂ ceramics, tuning and optimizing them for potential desired applications.

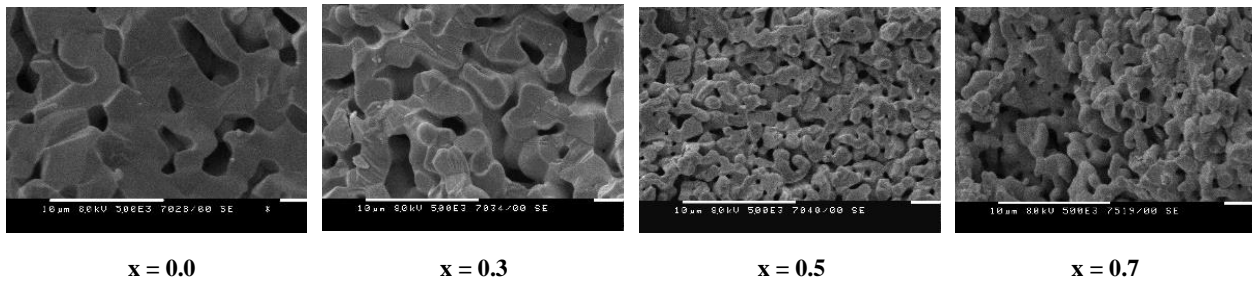


Figure 5. SEM pictures (cross section) of Ce_{1-x}Gd_xO_{2-x/2} samples, thermally treated at 1400 °C

3-3-FTIR Characterization

The infrared spectra of the Gd-doped CeO₂ powders (LT) and ceramics (HT), shown on Figure 6(a, b), are characterized by well pronounced band in the range 250 - 640 cm⁻¹, arising from the Ce-O and Gd-O stretching vibrations [24, 25]. This broad band becomes narrower in the ceramic samples, which could be explained by the high degree of crystallinity that is achieved as a result of the high temperature treatment. The observed weak band at around 880 cm⁻¹ could be ascribed to the formation of Na₂CO₃ [26]. The band disappears after the heat treatment at 1400 °C. The latter can be explained by the thermal decomposition of Na₂CO₃ into CO₂ and Na₂O, which takes place above 800 °C [27]. When temperature rises above 1275 °C, sodium oxide sublimates [28] explaining the absence of sodium in the final high-temperature material. The absorption band in the range 1360 - 1590 cm⁻¹ most probably originates from C=O vibrations issued by the carboxyl groups of the sodium alginate after decomposition during the thermal treatment at 500 degrees [26, 29].

The absorption band at around 3500 cm⁻¹ is assigned to the O-H stretching vibrations, probably arising from adsorbed moisture [30]. After calcination, most of the infrared absorption bands due to carbon-oxygen bonds disappear and only low-intensity O-H and metal-oxygen bond bands are detected.

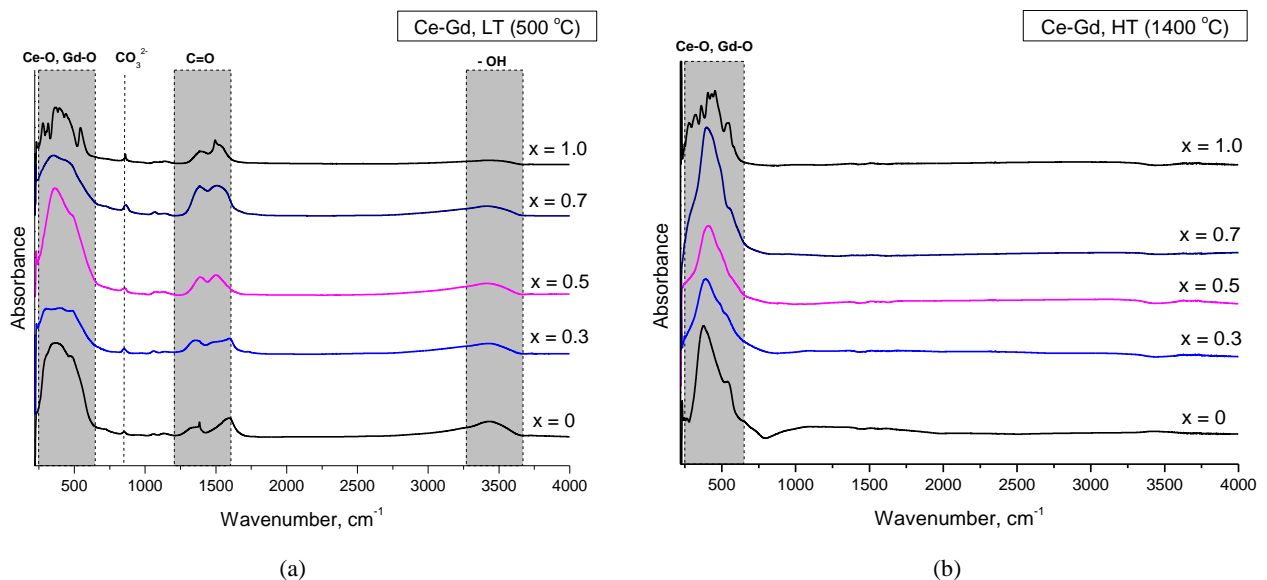


Figure 6. Infrared spectra of Ce_{1-x}Gd_xO_{2-x/2}: a) LT samples; b) HT samples

3-4-XPS Analysis

Figure 7 (a, b) presents Ce 3d photoemission spectra of Ce_{1-x}Gd_xO_{2-x/2}.

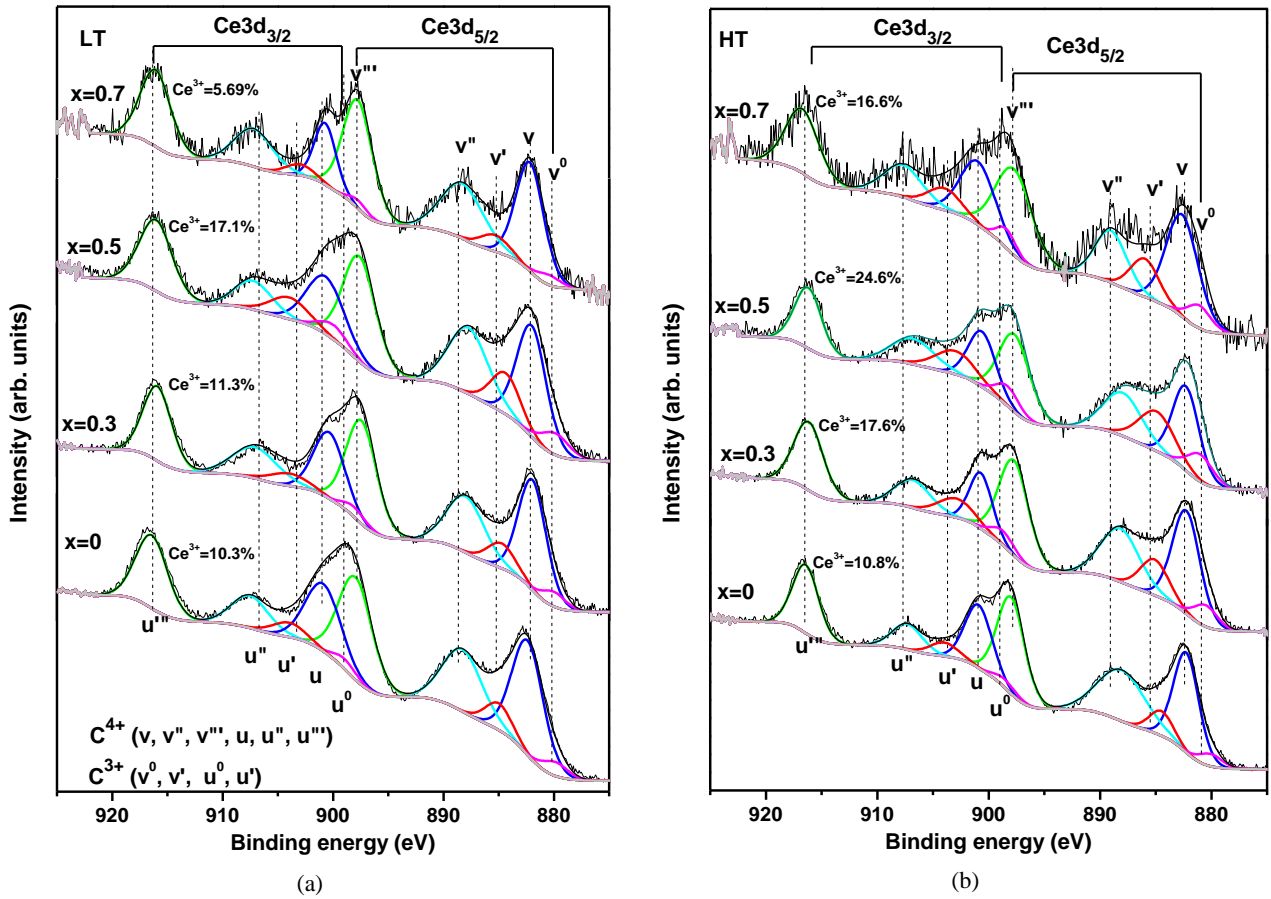


Figure 7. Ce 3d core-level spectra of $Ce_{1-x}Gd_xO_{2-x/2}$: a) LT samples; b) HT samples

There are six clearly visible peaks that are characteristic of CeO_2 and they correspond to three pairs of doublet lines which are due to different Ce 4f level occupancies in the different final electronic states of Ce^{4+} .

The deconvolution of the Ce 3d spectra was performed using the notations “v” and “u” introduced by Burroughs et al. [31] as presented in Figure 7. The components denoted as “v” correspond to the Ce $3d_{5/2}$ levels, while those denoted as “u” are assigned to the Ce $3d_{3/2}$ levels. The doublets labeled v-u and v''-u'' are attributed to the mixed $Ce3d^94f^1O2p^4$ and $Ce3d^94f^1O2p^5$ final states of Ce^{4+} . The doublet v'''-u''' arises from the $Ce3d^94f^0O2p^6$ final state of Ce^{4+} . Components v₀-u₀ and v'-u' correspond to $Ce3d^94f^2O2p^5$ and $Ce3d^94f^1O2p^6$ final states of Ce^{3+} , respectively. To detect the presence of Ce^{3+} , the Ce 3d spectra were fitted with five pairs of doublet lines. Ce^{4+} was fitted with three doublets, with the Ce $3d_{5/2}$ component positions being: v at 882.4 eV, v'' at 888.4 eV, and v''' at approximately 898.0 eV. The two additional doublets for Ce^{3+} have binding energies for Ce $3d_{5/2}$: v₀ at 880.2 eV and v' at 885.0 eV. Peak position constraints are ± 0.3 eV. The “u” components (Ce $3d_{3/2}$) are shifted by 18.4 eV to higher binding energies compared to the corresponding “v” components, with the intensity ratio A_u/A_v being 2/3.

The amount of Ce^{3+} in % is calculated by the formula:

$$Ce^{3+}[\%] = \frac{\sum A_{Ce^{3+}}}{\sum A_{Ce^{3d}}} \times 100\% \quad (1)$$

where $\sum A_{Ce^{3+}}$ is the sum of the v₀, u₀, v' and u' intensities and $\sum A_{Ce^{3d}}$ is the sum of the intensities of all ten Ce 3d components. The percentage values of the calculated quantities are given above the corresponding curves in Figure 7 (a, b).

Obviously, the calculated percentage of Ce^{3+} increases with the gadolinium content in both powders and ceramics, with a higher Ce^{3+} content observed in high-temperature (HT) samples compared to low-temperature (LT) ones. Surprisingly, in the low-temperature sample with $x = 0.7$, the amount of Ce^{3+} is the lowest. However, this observation might be misleading due to the reduced quality of the spectrum caused by the low cerium concentration. In contrast, the high-temperature sample with the same composition shows much more pronounced Ce^{3+} signal contributions. This is likely due to the formation of a more defect-free, homogeneous, and more ordered crystalline structure.

The O 1s spectra are shown in Figure 8(a, b). For the low-temperature (LT) samples, the O 1s spectra can be fitted with at least two distinct peaks (Figure 8a). The component with the lowest binding energy (BE) of 528.8–529.5 eV

corresponds to Ce-O and Gd-O bonds (lattice oxygen, OL-M-O). The O 1s component with a BE around 531–532 eV is attributed primarily to non-lattice oxygen (defect oxygen, OD), which arises from the creation of oxygen vacancies and defects in the crystalline structure. This component may also include contributions from adsorbed oxygen, impurities, or residuals from preparation procedures, such as cerium and gadolinium carbonates, OH-groups, etc. Peaks at BE > 532 eV are associated with adsorbed water from the atmosphere. Additionally, the Auger peak of sodium impurities, observed only in LT samples, is evident. This finding supports the FTIR observations. After high-temperature sintering (Figure 8b), the peak corresponding to lattice oxygen (OL) becomes the dominant and narrower peak, indicating the removal of residual products and the formation of a more homogeneous and well-defined crystalline structure.

The analysis of the oxidation state of gadolinium across the entire concentration range indicates that it remains in the 3+ oxidation state, as evidenced by the 3d (BE \approx 1187 eV) and 4d (BE \approx 143 eV) levels. However, a notable difference from pure oxidized gadolinium is the reduced binding energy of approximately 1 eV for the lower peak. This shift suggests a modification in the local environment around gadolinium, which provides evidence for its incorporation into the ceria lattice.

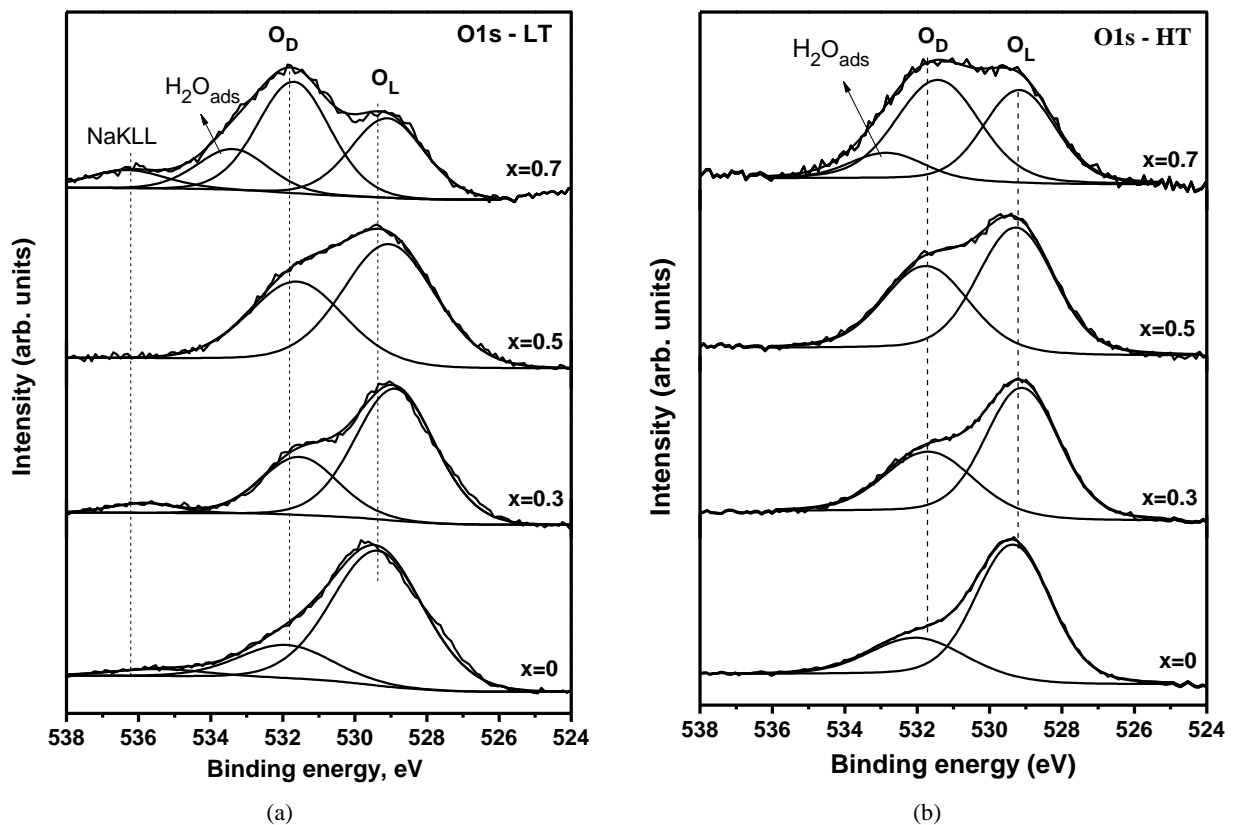


Figure 8. O 1s spectra of $Ce_{1-x}Gd_xO_{2-x/2}$: a) LT samples; b) HT samples

4- Conclusion

The impact of Gd doping in $Ce_{1-x}Gd_xO_{2-x/2}$ ($0 \leq x \leq 1$) solid solutions prepared by ionic gelation method with subsequent thermal treatment was determined over the entire range of gadolinium concentrations. It was found that the employed method for gadolinium incorporation in the ceria lattice yields stabilization of the crystal structure over a wider concentration range compared to alternative synthesis techniques. This was proven by the identified structural transformation from Fm-3m to Ia-3 space group, with specific gadolinium concentration threshold at $x \geq 0.4$ in the HT samples and $x \geq 0.7$ in the LT powders.

An evolution in the particle size was also observed, manifesting as a significant reduction in size with the increasing of gadolinium content. For the first time, high-temperature ceramics were prepared using powders synthesized by a low-temperature approach characteristic of the ionic gelation method. It provides new insights into the potential of the ionic gelation technique for creating advanced ceramic materials with enhanced thermal stability.

The results included in this study indicate the utility of gadolinium doping to modify the structure and, respectively, properties of CeO_2 ceramics in order to facilitate state-of-the-art applications. For example, development of electrolyte materials for solid oxide fuel cells, where the presence of Ce^{3+} contributes significantly to improving ionic conductivity, facilitating oxygen reduction, and reducing cell operating temperatures.

5- Declarations

5-1-Author Contributions

Conceptualization, V.I. and T.P.; methodology, V.I., V.B., and N.B.; software, G.A. and E.L.; validation, H.K., G.A., O.D., and E.L.; formal analysis, V.B., T.P., and V.I.; investigation, V.B., O.D., and V.I.; resources, T.P.; data curation, G.A., O.D., and E.L.; writing—original draft preparation, T.P.; writing—review and editing, V.I., O.D., and V.B.; visualization, V.I., O.D., V.B., and T.P.; supervision, T.P.; project administration, T.P. and V.I.; funding acquisition, T.P. All authors have read and agreed to the published version of the manuscript.

5-2-Data Availability Statement

Data sharing is not applicable to this article.

5-3-Funding and Acknowledgements

The authors appreciate the financial support of the Bulgarian National Science Fund under contract KII 06-H59/13.

5-4-Institutional Review Board Statement

Not applicable.

5-5-Informed Consent Statement

Not applicable.

5-6-Conflicts of Interest

The authors declare that there is no conflict of interest regarding the publication of this manuscript. In addition, the ethical issues, including plagiarism, informed consent, misconduct, data fabrication and/or falsification, double publication and/or submission, and redundancies have been completely observed by the authors.

6- References

- [1] Choolaeia, M., Caia, Q., Sladeb, R.C.T., Horri, B.A. (2018). Nanocrystalline gadolinium-doped ceria (GDC) for SOFCs by an environmentally-friendly single step method. *Ceramics International*, 44, 13286 - 13292. doi:10.1016/j.ceramint.2018.04.159.
- [2] Shah, M.A.K., Lu, Y., Mushtaq, N., Yousa, M., Lund, P., Asghar, M.I., Zhu, B. (2023). Designing Gadolinium-doped ceria electrolyte for low temperature electrochemical energy conversion. *International Journal of Hydrogen Energy*, 48(37), 14000-14011. doi:10.1016/j.ijhydene.2022.12.314.
- [3] El-Habib, A., Brioual, B., Zimou, J., Rossi, Z., Marjaoui, A., Zanouni, M., Aouni, A., Jbilou, M., Diani, M., Addou, M. (2024). Comparative studies on the structural, optical and electrochemical properties of Gd, Nd and In-doped CeO₂ nanostructured thin films. *Materials Science in Semiconductor Processing*, 176, 108287. doi:10.1016/j.mssp.2024.108287.
- [4] Inaba, H., Tagawa, H. (1996). Ceria-based solid electrolytes. *Solid State Ionics*, 83(1-2), 1-16. doi:10.1016/0167-2738(95)00229-4.
- [5] Momin, N., Manjanna, J., Senthilkumar, S., Aruna, S.T. (2022). La-and Gd-Doped CeO₂ Nanoparticles as Electrolyte Materials for Intermediate Temperature Solid Oxide Fuel Cells. *Recent Trends in Electrochemical Science and Technology. Springer Proceedings in Materials*, Volume 15, Springer, Singapore. doi:10.1007/978-981-16-7554-6_10.
- [6] Wang, K., Yang, J., An, B., Zhang, Q., Song, D., & Wang, Y. (2024). Mechanical and electrical properties Ge and Gd co-doped CeO₂-based electrolyte for intermediate-temperature solid oxide fuel cells. *Ceramics International*, 50(20), 37698-37713. doi:10.1016/j.ceramint.2024.07.131.
- [7] Zhu, M., Du, C., Zhou, R., Li, D., Wang, S., Tian, C., & Chen, C. (2024). Synthesis and characterization of Ce_{1-x}(Gd_{1/5}Sm_{1/5}Er_{1/5}Y_{1/5}Bi_{1/5})xO_{2-δ} solid electrolyte for SOFCs. *Journal of Rare Earths*. doi:10.1016/j.jre.2024.03.002.
- [8] Sun, Q., Fu, Zh., Yang, Z. (2018) Effects of rare-earth doping on the ionic conduction of CeO₂ in solid oxide fuel cells. *Ceramics International*, 44(4), 3707-3711. doi:10.1016/j.ceramint.2017.11.149.
- [9] Fuentes, R. O., Baker, R. T. (2008). Synthesis and properties of Gadolinium-doped ceria solid solutions for IT-SOFC electrolytes. *International Journal of Hydrogen Energy*, 33(13), 3480-3484. doi:10.1016/j.ijhydene.2007.10.026.
- [10] Kalinina, M., Dyuskina, D., Mjakin, S., Kruchinina, I., Shilova, O. (2023). Comparative Study of Physicochemical Properties of Finely Dispersed Powders and Ceramics in the Systems CeO₂-Sm₂O₃ and CeO₂-Nd₂O₃ as Electrolyte Materials for Medium Temperature Fuel Cells. *Ceramics*, 6(2), 1210-1226. doi:10.3390/ceramics6020073.

- [11] Wu, Y.-C., Lin, C.-C. (2014). The microstructures and property analysis of aliovalent cations (Sm^{3+} , Mg^{2+} , Ca^{2+} , Sr^{2+} , Ba^{2+}) co-doped ceria-base electrolytes after an aging treatment. *International Journal of Hydrogen Energy*, 39, 7988-8001. doi:10.1016/j.ijhydene.2014.03.063.
- [12] Tompsett, G.A., Sammes, N. M. (1997). Ceria–Yttria-Stabilized Zirconia Composite Ceramic Systems for Applications as Low-Temperature Electrolytes. *Journal of the American Ceramic Society*, 80(12), 3181–86. doi:10.1111/j.1151-2916.1997.tb03247.x.
- [13] Li, P., Chen, X., Li, Y., Schwank, J. W. (2019). A review on oxygen storage capacity of CeO_2 -based materials: Influence factors, measurement techniques, and applications in reactions related to catalytic automotive emissions control. *Catalysis Today*, 327, 90-115. doi:10.1016/j.cattod.2018.05.059.
- [14] Swathi, S., Yuvakkumar, R., Senthil Kumar, P., Ravi, G., Thambidurai, M., Dang, C., Velauthapillai, D. (2023). Gadolinium doped CeO_2 for efficient oxygen and hydrogen evolution reaction. *Fuel*, 310, Part A, 122319. doi:10.1016/j.fuel.2021.122319.
- [15] Kim, M., Park, G., Jo, K., Lee, H. (2023). Enhanced redox properties of Gd-doped CeO_2 - TiO_2 induced by oxygen vacancies and disordered structure. *Materials Today Chemistry*, 29, 101440. doi:10.1016/j.mtchem.2023.101440.
- [16] Trovarelli, A. (1996). Catalytic Properties of Ceria and CeO_2 -Containing Materials. *Catalysis Reviews*, 38(4), 439-520. doi:10.1080/01614949608006464.
- [17] Bhalkikar, A., Wu, T.-S., Fisher, T. J., Sarella, A., Zhang, D., Gao, Y., Soo, Y.-L., Cheung, C. L. (2020). Tunable catalytic activity of gadolinium-doped ceria nanoparticles for pro-oxidation of hydrogen peroxide. *Nano Research*, 13, 2384–2392. doi:10.1007/s12274-020-2861-2.
- [18] Hernández, M. Y., Laguna, O. H., Centeno, M. A., Odriozola, J. A. (2011). Structural and catalytic properties of lanthanide (La, Eu, Gd) doped ceria. *Journal of Solid-State Chemistry*, 184(11), 3014-3020. doi:10.1016/j.jssc.2011.09.018.
- [19] Pezeshkpour S., Abdullah A. Z., Salamatinia B., Horri B. A., B. (2017). Ionic–gelation synthesis of gadolinium doped ceria ($\text{Ce}_{0.8}\text{Gd}_{0.2}\text{O}_{1.90}$) nanocomposite powder using sodium-alginate, *Ceramics International*, 43 (9), 7123-7135. doi:10.1016/j.ceramint.2017.02.145.
- [20] Wang, Z., Kale, G. M., Ghadiri, M. (2012). Synthesis and characterization of $\text{Ce}_x\text{Gd}_{1-x}\text{O}_{2-\delta}$ nanopowders employing an alginate mediated ion-exchange process. *Chemical Engineering Journal*, 198–199, 149-153. doi:10.1016/j.cej.2012.05.063.
- [21] Pawley, G. S. (1981). Unit-cell refinement from powder diffraction scans. *Journal of Applied Crystallography*, 14, 357-361. doi:10.1107/S0021889881009618.
- [22] Grover, V., Tyagi, A. K. (2004). Phase relations, lattice thermal expansion in CeO_2 - Gd_2O_3 system, and stabilization of cubic gadolinia. *Materials Research Bulletin*, 39, 859-866. doi:10.1016/j.materresbull.2004.01.007.
- [23] Momma, K., Izumi, F. (2011). VESTA 3 for three-dimensional visualization of crystal, volumetric and morphology data. *Journal of Applied Crystallography*, 44, 1272-1276. doi:10.1107/S0021889811038970.
- [24] Arabaci, A. (2015). Effect of Sm and Gd dopants on structural characteristics and ionic conductivity of ceria. *Ceramics International*, 41, 5836-5842. doi:10.1016/j.ceramint.2015.01.013.
- [25] Rocha, R. A., Muccillo, E. N. S. (2003). Physical and chemical properties of nanosized powders of gadolinia-doped ceria prepared by the cation complexation technique. *Materials Research Bulletin*, 38, 1979-1986. doi:10.1016/j.materresbull.2003.09.025.
- [26] Araújo, P. S., Belini, G. B., Mambrini, G. P., Fabio, M. Y., Waldman, W. R. (2019). Thermal degradation of calcium and sodium alginate: A greener synthesis towards calcium oxide micro/nanoparticles. *International Journal of Biological Macromolecules*, 140, 749-760. doi:10.1016/j.ijbiomac.2019.08.103.
- [27] Newkirk, A. E., Ifigenia, A. (1958). Drying and Decomposition of Sodium Carbonate. *Analytical Chemistry Journal*, 30, 982-984. doi:10.1021/ac60137a031.
- [28] Weast, R.C. (1985). *Handbook of Chemistry and Physics*. CRC Press, Boca Raton, United States.
- [29] Pathak, T. S., Yun, J. H., Lee, S. J., Baek, D. J., Paeng, K. J. (2010). Effect of solvent composition on porosity, surface morphology and thermal behavior of metal alginate prepared from algae (*Undaria pinnatifida*). *Journal of Polymers and the Environment*, 18, 45–56. doi:10.1007/s10924-009-0156-5.
- [30] Ankita, C. S., Singh, S., Kumar, L., Gupta, V., Kumar, S., Kumar, S, Kumar, P. (2024). Gd doped Cerium Oxide for organic dye degradation and tuning of magnetic properties. *Materials Science and Engineering: B*, 300, 117049. doi:10.1016/j.mseb.2023.117049.
- [31] Burroughs, P., Hamnett, A., Orchard, A. F., Thornton, G. (1976). Satellite structure in the X-Ray photoelectron spectra of some binary and mixed oxides of lanthanum and cerium. *Journal of the Chemical Society, Dalton Transactions*, 17, 1686-1698. doi:10.1039/DT9760001686.